

Article

Evaluation of Counter-Rotating Dual-Rotor Permanent-Magnet Flux-Switching Machine with Series and Parallel Stator Teeth

Wasiq Ullah ^{1,*}, Faisal Khan ^{1,*}, Udochukwu Bola Akuru ², Bakhtiar Khan ³ and Salar Ahmad Khalil ⁴

¹ Electric Machine Design Research Lab, Department of Electrical and Computer Engineering, COMSATS University Islamabad, Abbottabad Campus Abbottabad, Abbottabad 22060, Pakistan

² Department of Electrical Engineering, Tshwane University of Technology, Pretoria 0183, South Africa; AkuruUB@tut.ac.za

³ Department of Electrical Engineering, Karakoram International University, Gilgit 15100, Pakistan; engr.bakhtiar.khan@gmail.com

⁴ Department of Electrical Engineering (Power), USPCAS-E, National University of Science and Technology, Islamabad 24090, Pakistan

* Correspondence: wasiqullah014@gmail.com (W.U.); faisalkhan@cuiatd.edu.pk (F.K.); Tel.: +92-30-2886-2038 (W.U.)

Abstract: In this study, the focus is on the magnetic path formation and its effects on the performance of a counter-rotating dual-rotor permanent-magnet flux-switching machine (CR-DRPMFSM) for direct-drive counter-rotating wind power generation, based on different stator slot and rotor pole combinations. To fully exploit rotor-shaft bore and improve fault-tolerant design, as well as increase torque density, dual-rotor topologies with the capability for dual electrical and dual mechanical ports are investigated. Moreover, the direct-drive counter-rotating wind power generation technique offers a brushless topology, thus reducing maintenance cost and improving energy conversion efficiency compared to single-blade wind turbine systems. Using finite element analysis (FEA), the inherent magnetic coupling of the series and parallel paths shows varied impacts on the electromagnetic performance of four different CR-DRPMFSMs based on the slot/pole combinations (MI to MIV) considered in this study. The key electromagnetic performance indices, such as torque, cogging torque, torque ripple, power factor, and efficiency, show proportionate variation to the coupling level. A comparative analysis shows that MI exhibits higher average torque, lower torque ripples, and high efficiency, reaching 90% with a power factor of 0.6. As an optimal design, an MI test prototype is developed. The experimental test prototype validates the FEA results under no-load and on-load conditions.

Keywords: dual-rotor flux-switching machine; counter-rotating; magnetic coupling; permanent magnet; wind power generation



Citation: Ullah, W.; Khan, F.; Akuru, U.B.; Khan, B.; Khalil, S.A. Evaluation of Counter-Rotating Dual-Rotor Permanent-Magnet Flux-Switching Machine with Series and Parallel Stator Teeth. *Machines* **2023**, *11*, 989. <https://doi.org/10.3390/machines11110989>

Academic Editor: Ahmed Abu-Siada

Received: 4 October 2023

Revised: 21 October 2023

Accepted: 23 October 2023

Published: 26 October 2023



Copyright: © 2023 by the authors. Licensee MDPI, Basel, Switzerland. This article is an open access article distributed under the terms and conditions of the Creative Commons Attribution (CC BY) license (<https://creativecommons.org/licenses/by/4.0/>).

1. Introduction

Due to their high torque density and compact construction, dual-mechanical- and electrical-port machines have recently attracted research interests. To this end, unique machines with simple, sturdy structures and high torque and power densities, such as dual-rotor permanent-magnet flux-switching machines (DRPMFSMs), have been proposed [1–5]. Two rotors, the inner and outer rotors, sandwich a single stator in the structure of DRPMFSMs. As a result, machine performance, particularly torque, is enhanced.

On the other hand, due to concerns about the cost of PM materials, recent studies have considered magnet-less variants of dual-rotor machines to cut down on hardware cost while boosting the torque density based on the so-called brushless stator-mounted wound-field flux-switching machines [6]. In addition, flux controllability of magnet-less dual-rotor flux-switching machines makes it attractive for specific application areas [7,8]. Notwithstanding, DRPMFSMs are comparatively preferred to their wound-field variants since they eliminate

field copper losses present in wound-field designs, potentially improving efficiency. In addition, DRPMFMSMs enable high air-gap flux density and torque density capabilities. Even when compared to high-temperature superconducting (HTS) dual-rotor flux-switching machines [9], DRPMFMSMs are more cost effective for the same performance, while offering better temperature capabilities than HTSs which require cryogenic cooling since PMs can operate at higher temperatures. However, because of the structure's high degree of integration, there are mutual electromagnetic effects such as magnetic field coupling between the inner and outer machines' fields.

There are numerous studies conducted on dual-rotor permanent-magnet (DRPM) machines to reduce the non-negligible impacts of magnetic coupling effects. Design-wise, the flux-weakening effects of magnetic coupling can possibly be mitigated by choosing the right design topologies, such as unique PM structures [10] or different winding configurations [11]. The authors of [12] also adopted a novel control strategy as a means of suppressing the detrimental magnetic coupling effects.

In [13], the magnetic coupling consequence is examined from the standpoint of airgap harmonic groups in the context of DRPMFMSMs, with the main emphasis on the effects of the positive and negative coupling harmonics and how they affect torque performance, back-EMF, and overload capacity. This study, however, does not consider various stator slot and rotor pole combinations.

With an emphasis on PM field distribution, back-EMF and air-gap flux density between the inner and outer stator tooth numbers, the effect of magnetic coupling on co-axial DRPMFMSMs is explored in [14] for hybrid electric vehicles. This study does not provide any information available on the impact on other electromagnetic performance indices, such as power factor, torque, efficiency, and torque ripple. In summary, a comparative analysis on the shortcomings of existing dual-rotor machine winding topologies is provided in Table 1.

Table 1. Comparison of dual-rotor topologies.

Refs.	Winding	Shortcomings and Comments
[2]	Drum winding	Mechanically coupled rotor and, therefore, counter rotation is not possible. Mutual coupling effect exists but is not analyzed.
[6]	Concentrated toroidal winding	Pancake structure and, therefore, is not feasible for counter rotation. Integral rotor structure by mechanically coupling of inner and outer rotor with end disc
[7]	Group concentrate for armature winding and toroidal winding for field excitation	Mechanically coupled rotor and, therefore, counter rotation is not possible. Due to group winding, the magnetic path formed is longer. As a result of armature winding groups, the mutual effect is higher.
[9]	Toroidal field winding Armature winding overlapped field coils	Modular segmented stator creates manufacturing complexity. High-temperature superconductor (HTS) winding is adopted and, therefore, requires cryogenic cooling.

Therefore, to the best of the authors' knowledge and based on the existing literature, information about magnetic coupling effects on the electromagnetic performance of the series and parallel teeth of DRPM machines is still lacking, particularly for counter-rotating DRPMFMSMs (CR-DRPMFMSMs) designed for direct-drive wind power generation systems, as illustrated in Figures 1 and 2. The proposed CR-DRPMFMSM design employs concentrated dual armature windings with low-cost ferrite PMs, which are both housed on a single stator. The stator is positioned between the inner and outer rotors which rotate in opposite directions. The proposed CR-DRPMFMSM has a unique mechanical assembly, as illustrated in Figure 1b, which produces counter rotation via its dual rotors.

The proposed evaluation of the magnetic coupling effects in CR-DRPMFMSMs is important due to the following reasons:

- With a complex magnetic topology due to the two rotors, the interactions between the flux sources and circulating fluxes are also complicated and not yet explored.

- The magnetic coupling between the stator and two rotors, as well as between the series and parallel teeth, could have significant impacts on torque production, cogging torque, torque ripple, losses, etc.
- The counter-rotating (CR) topology brings additional challenges and degrees of freedom that require dedicated analysis.
- With a better understanding, CR-DRPMFSMs can be designed to maximize power density, efficiency, and reliability.
- The knowledge gained would be applicable to other complex multi-rotor and flux-modulation machine topologies.
- There are practical economic and technological benefits for the proposed direct-drive wind power generation systems which utilize high-torque-density machines.

For the rest of the paper, Section 2 is used to discuss the characteristics of wind power generation, while Section 3 is focused on the results and discussion on the electromagnetic performance study based on different slot/pole configurations. This leads to an experimental study to confirm the validity of the proposed design and the accuracy of the FEA predicted results. In the end, some conclusions are drawn in Section 4.

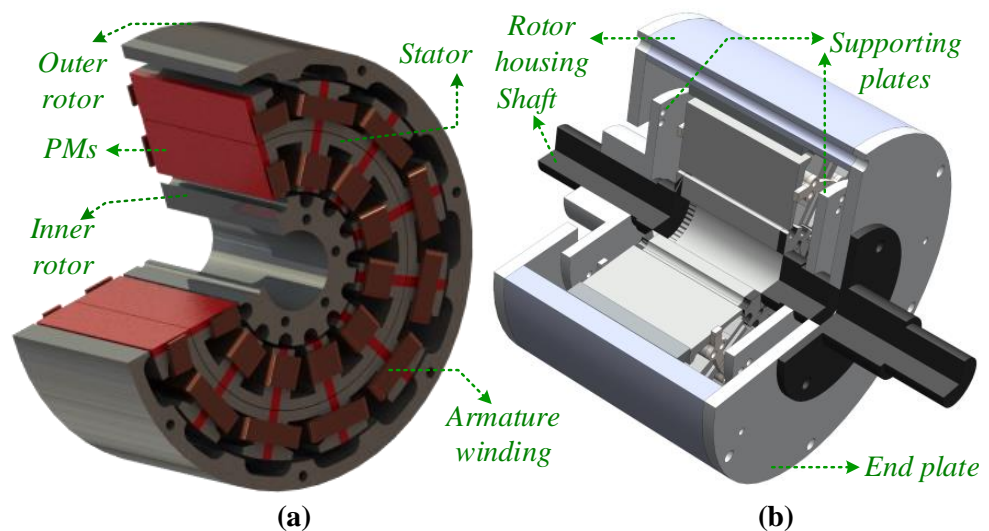


Figure 1. Proposed design: (a) 3D view, and (b) mechanical assembly.

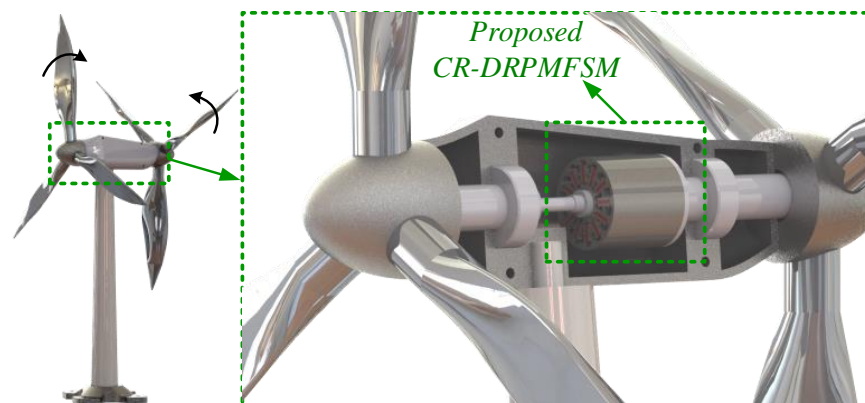


Figure 2. Direct-drive counter-rotating wind power generation [15].

2. Characteristics of Wind Power Generation

2.1. Direct Drive Counter-Rotating Wind Power Generation

A pair of wind blades are attached to a dual-rotor wind turbine, which rotate in the opposite direction. A type of dual-rotor wind turbine used to produce wind energy is the

direct-drive counter-rotating wind turbine (DDCRWT). As previously stated, the proposed CR-DRPMFSM in DDCRWTs comprise double rotors, i.e., inner and outer rotors, whose shafts are then united to the DDCRWT gearless system as shown in Figure 2. It is evident that in the case of DDCRWTs, the inner rotor of the proposed CR-DRPMFSM rotates in a clockwise direction while being directly coupled with the shaft of the front wind turbine. On the other hand, the outer rotor turns anticlockwise while being connected to the blades of the rear wind turbines.

Since a DDCRWT generates more power compared to a single-rotor wind turbine or dual-rotor co-rotating system, it is prioritized for the proposed CR-DRPMFSG. To this end, effectiveness is examined in-depth in terms of slot/pole combinations and magnetic coupling for the series and parallel teeth's magnetic paths based on finite element analysis (FEA) and experimental methods.

2.2. Magnetization Concept for Series and Parallel Stator Teeth

In the ideal single air-gap case, possible slot/pole combinations are not perturbed by magnetic coupling effects. However, due to the tangentially magnetized sandwiched PMs in the parallel-tooth design, there is a coupling phenomenon. For least magnetic coupling, the possible stator slot/rotor pole combinations that form the series and parallel stator teeth are derived as follows:

$$\begin{cases} N_{so} = kN_{sin} \\ N_{so} = nN_{sin} \end{cases} \quad \text{and} \quad \begin{cases} N_{ro} = N_{so} \left(2 \pm \frac{k}{2m}\right) \\ N_{rin} = N_{sin} \left(2 \pm \frac{k}{2m}\right) \end{cases} \quad (1)$$

where N_{so} is the inner machine stator teeth and N_{sin} is the outer machine stator teeth. Similarly, N_{ro} is the outer machine rotor pole number, and N_{rin} is the inner machine rotor pole number. Furthermore, n is a fractional number, m defines the number of phases, and k is a positive integer.

Based on the above-mentioned formulation and geometric derivation, the relations of the stator teeth between the inner and outer rotors are defined as parallel, series, and independent, as shown in Figure 3. In the case when stator teeth between the upper and lower slots are in line and the magnetization direction of both PMs is the same (as shown in Figure 3a), then the stator teeth formed are parallel stator teeth due to parallel magnet path formation. Similarly, when the stator teeth are in line, but the magnetization direction of the upper and lower PMs is in the reverse direction (as shown in Figure 3b), then the magnetic path formed is series, and the stator teeth are termed series stator teeth. Finally, when one of the stator teeth is in line with the other stator teeth in the middle of the stator (as shown in Figure 3c), then the magnetic flux path formed is independent and the stator teeth are termed independent teeth. Based on the slot/pole combinations between the inner and outer stator teeth, the magnetic path and, hence, the stator teeth vary, resulting in greatly varying overall electromagnetic performance.

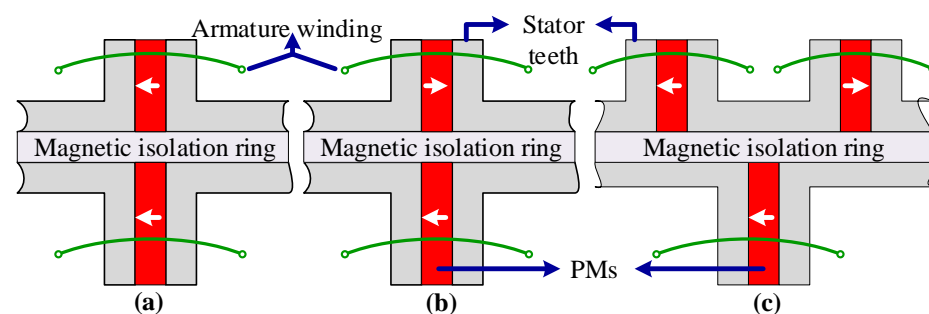


Figure 3. Stator teeth formation in CR-DRPMFSM: (a) parallel teeth (b) series teeth, and (c) independent teeth.

Thus, to investigate the impact of series, parallel, and independent stator teeth, various slot/pole combinations for the inner and outer machines were opted for as case studies, among which four dominant cases, including 12S/14P-12S/14P (termed MI), 6S/5P-18S/42P (MII), 6S/5P-12S/22P (MIII), and 12S/10P-12S/22P (MIV), are shown in Figure 4 with their distinct magnetic path formations and magnetic flux paths.

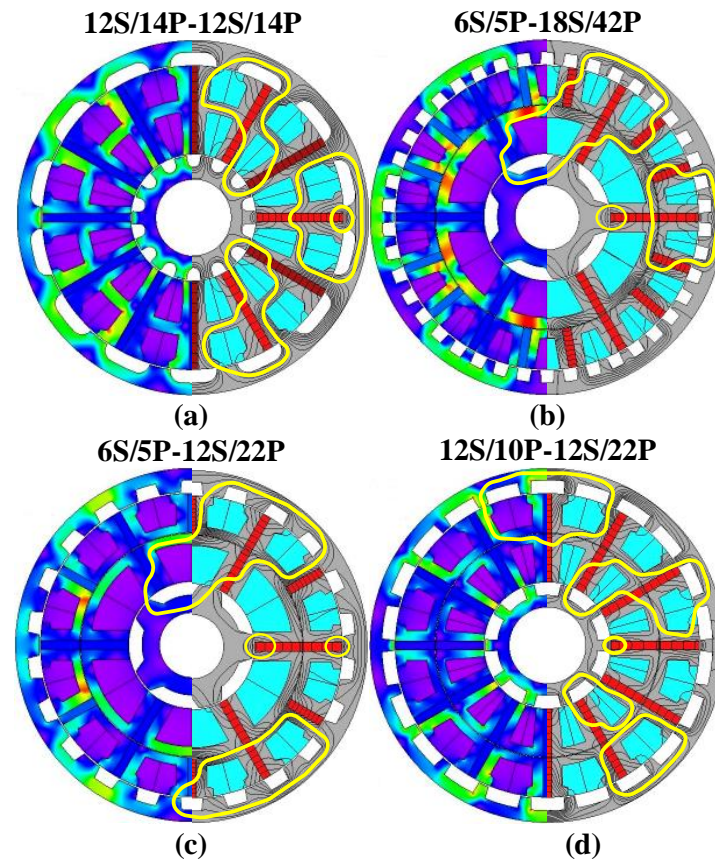


Figure 4. Magnetic flux density (left half of machines), magnetic flux lines (right half of machines) and magnetic flux path (yellow line loops) for stator teeth with different slot/pole combinations: (a) MI, (b) MII, (c) MIII, and (d) MIV.

Based on the flux path and magnetic circuit, the structure MI (as shown in Figure 4d) forms a parallel magnetic circuit path due to the alignment of the stator teeth in line, whereas between the inner and outer stators, some series circuit is also established with flux circulation. For MII, the slot/pole combination of the inner and outer machines is 6S/5P-18S/42P, as shown in Figure 4b. It is evident that all the inner stator teeth form parallel teeth, whereas in the outer stator, phase A forms parallel and phase B/C form independent teeth. In addition, the inner parallel teeth with all the outer independent teeth of phase B/C form a sort of PI-type series magnetic circuit. For MIII, the slot/pole combination of the inner and outer machines is 6S/5P-12S/22P, as shown in Figure 4c. It can be clearly seen that inner series and parallel teeth are formed in the inner stator, whereas series, parallel, and independent teeth are formed in the outer stator. Moreover, the inner and outer series form a sort of series–series magnetic circuit, whereas the inner series with the outer independent teeth result in a PI-type series magnetic circuit. It is important to note that for MII and MIII topologies, a series magnetic circuit is generated with the nearest inner parallel stator teeth. Finally, structure MIV (as shown in Figure 4d) is formed from the combination of a very common structure, i.e., 12 slots/10 poles and 12 slots/22 poles, for optimal topology. Based on the magnetic circuit formation, it is evident that a parallel magnetic circuit path is developed in the inner and outer stators, while a series circuit is also established.

Based on the formation of series, parallel, and independent stator teeth, the PM coupling and magnetic flux density (as shown in Figure 5) greatly varies, resulting in the overall electromagnetic performance being affected. Thus, to find the optimal design with the least PM coupling and better electromagnetic performance, a detailed performance analysis is presented in the proceeding section.

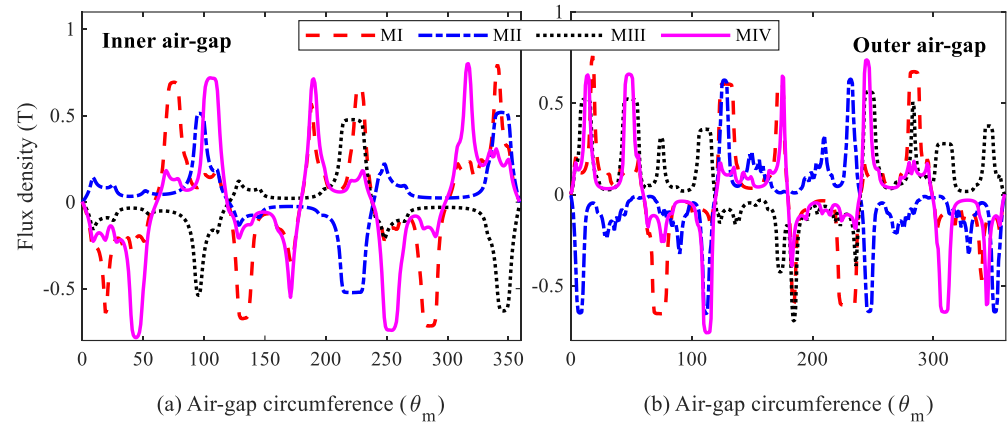


Figure 5. Air-gap flux density distribution: (a) inner air gap, and (b) outer air gap.

3. Results and Discussion

3.1. Electromagnetic Performance Analysis

In this section, the FEA technique is used to evaluate the magnetic coupling impact of the series and parallel teeth on the highlighted machines in Figure 4. Since the proposed CR-DRPMFSMs combine the inner machine (inner stator and rotor) and outer machine (outer stator and rotor), and due to the dual-port feature, the impact on individual machine inner and outer ports was investigated. This detailed investigation included both no-load and on-load profiles.

An analysis of the inner-port flux linkage, as shown in Figure 6a, shows that MI, followed by MIV, MII, and MIII, offers maximum flux. The maximum flux offered by MI is due to its lower magnetic coupling compared to the other designs. Additionally, due to the highest magnetic coupling between the inner and outer machines in MIII, the corresponding flux linkage is adversely affected in the form of a drop in the amplitude. Furthermore, from the harmonic spectra shown in Figure 6b, it is clearly shown that MIV offers the highest fundamental component; however, due to the dominance of higher-order harmonics, the peak-to-peak values are adversely impacted. Moreover, in terms of higher-order harmonics, the least harmonics are offered by MI, whereas the rest exhibit dominant odd-order harmonics and minor even-order harmonics as well. In the same way, both MI and MIV outer ports offer approximately maximum flux, followed by MII and MIII, as shown in Figure 6c. The reduction in the peak-to-peak flux linkage magnitude of MI arises due to the higher-order harmonic content, as exhibited in Figure 6d. The 5th harmonic order, which is dominant, results in a reduction in the magnitude of the fundamental component. This is due to variation in the magnetic flux density of the series, parallel, and independent stator teeth.

The back-EMF waveform and magnitude of harmonic spectra greatly differ due to the inconsistency of coupling through the series, parallel, and independent stator teeth for all topologies, as shown in Figure 7. It is interesting to notice that although the behavior of the back-EMF waveforms for the inner and outer machines are roughly sinusoidal, their harmonic spectra exhibit both even and odd higher-order harmonic orders due to the dominance of coupling.

For the inner machine in Figure 7a,b, MI and MIV demonstrate good-quality sinusoidal back-EMF waveforms with a higher magnitude compared to MII and MIII. This is because MII and MIII show lower fundamental components, while MIII also suffers from the impact of higher-order harmonics. Additionally, in the case of the outer ports, as shown

in Figure 7c,d, it can be seen that MIII yields a distorted back-EMF profile compared to the other topologies which are approximately sinusoidal, with the highest magnitude from MII, followed by MI and MIII. However, due to the coupling effect of the series, parallel, and independent stator teeth between the inner and outer ports, there exist even-order harmonics.

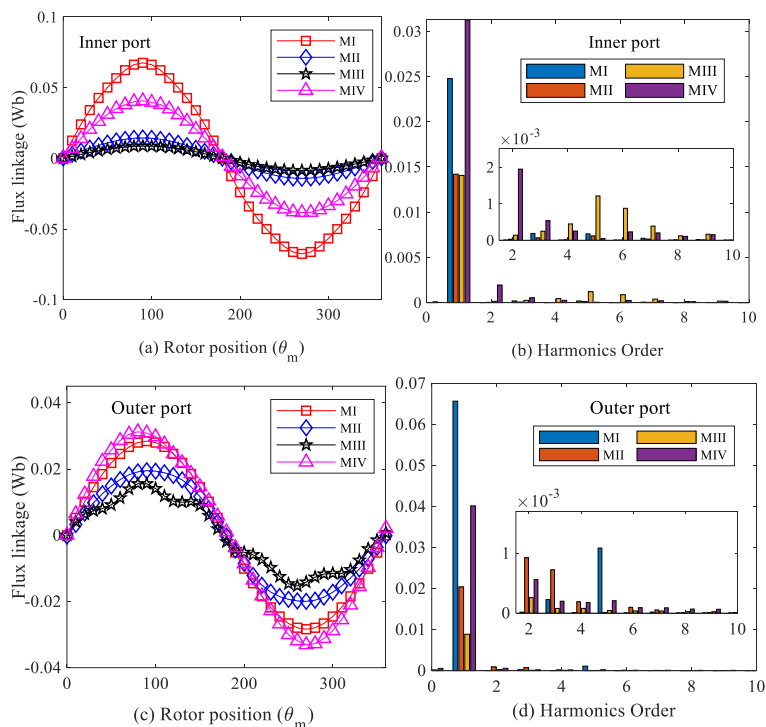


Figure 6. No-load flux linkage: (a) inner-port waveform, (b) inner-port harmonic spectra, (c) outer-port waveform, and (d) outer-port harmonic spectra.

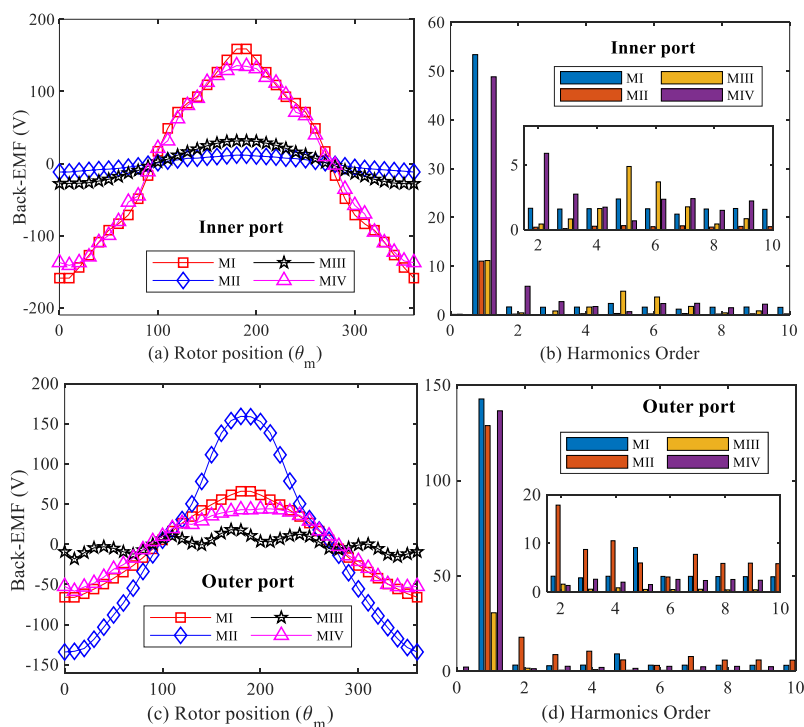


Figure 7. Back-EMF: (a) inner-port waveform, (b) inner-port harmonic spectra, (c) outer-port waveform, and (d) outer-port harmonic spectra.

Under on-load conditions, the selected CR-DRPMFSMs were examined at different operating conditions to strictly explore the impact of series and parallel stator teeth on electromagnetic performance. In this regard, detailed analysis of the key performance indicators, including copper losses, average torque, total machine losses, ripple rate, power factor, output power, and efficiency, were accomplished.

To assess overload capabilities, the initially designed CR-DRPMFSM was run at various current densities. The average torque profiles under varying current density shown in Figure 8 demonstrate that magnetic coupling and variation through the series and parallel stator teeth cause not only the average torque but also the overload capability of the inner and outer ports to substantially vary. In the case of the inner port, as shown in Figure 8a, it is evident that MI offers the highest average torque, followed by MIV, whereas MII and MIII show a similar response with low overload capability. Similarly, the torque and overload behavior of the outer port (as shown in Figure 8b) reveal interesting results. It can be clearly seen that MIV shows slightly higher torque than MI and the same overload capability, whereas the overload profile of MII is excellent. It was found that MI is the most appropriate design that exhibits the highest average torque by comparing the average torque of the inner and outer ports in the selected case studies. Additionally, to avoid saturation and achieve maximum torque, 15 A/mm^2 was found to be the optimum current density.

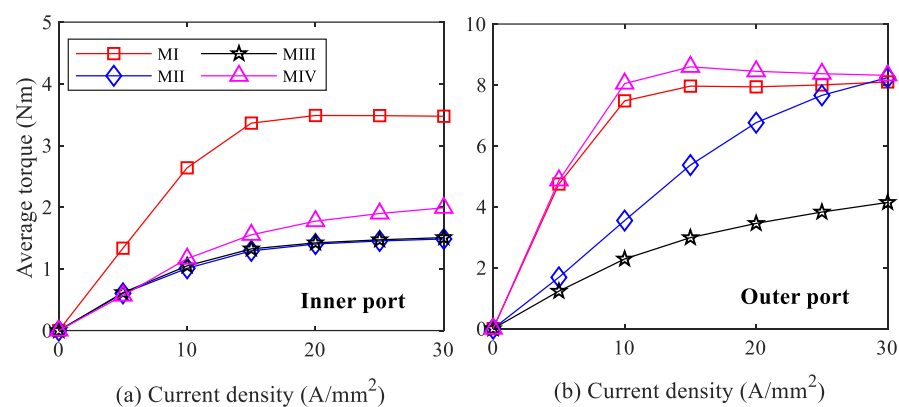


Figure 8. Average torque of (a) inner port and (b) outer port.

Series and parallel alignments of the stator teeth have a dominant impact on magnetic coupling, which impacts the back-EMF in the form of odd and even higher-order harmonics. In terms of the rate of torque ripples, the 5th- and 7th-order harmonics have a significant impact on the torque profile. Figure 9 depicts the effect of torque ripples on the average torque for both the inner and outer ports. The analysis demonstrates that for both the inner and outer ports, the ripple rate and average torque increase proportionately, but at a different increasing rate. Figure 9a demonstrates that in the case of the inner port, the lowest ripple rate is offered by MI and the highest is offered by MIV, whereas MII and MIII show a comparatively lower ripple rate but also exhibit lower torque. Similarly, Figure 9b shows for the outer port machines that torque ripple in MI decreases with an increase in average torque, while MII suffers from very high ripple rates.

To evaluate the efficient functioning of the proposed machines and selection of the best design for prototype construction, efficiency was assessed against output power, as indicated in Figure 10. In the case of the inner port, as shown in Figure 10a, it is seen that the maximum output power and efficiency are achieved by MI, followed by MIV, in both the inner and outer ports, whereas MII and MIII show the worst response in the inner port. In the outer port, MII has a comparatively better response than MIII but not better than MI and MIV. Based on the analysis, it is evident that among all topologies, MI is optimal for comparatively better efficiency and output power.

To ensure high efficiency at the peak power factor, all topologies were examined, as shown in Figure 11. For both the inner and outer ports, the analysis shows that for the inner

port, MIII exhibits a higher power factor while MI displays higher efficiency. Similarly, in the case of the outer port, MI, MII, and MIV show high efficiency and a good power factor.

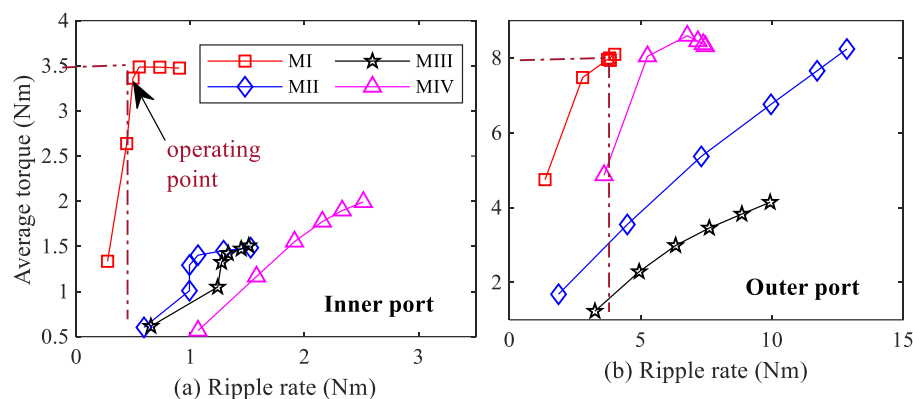


Figure 9. Impact of torque ripple rate on average torque: (a) inner port and (b) outer port.

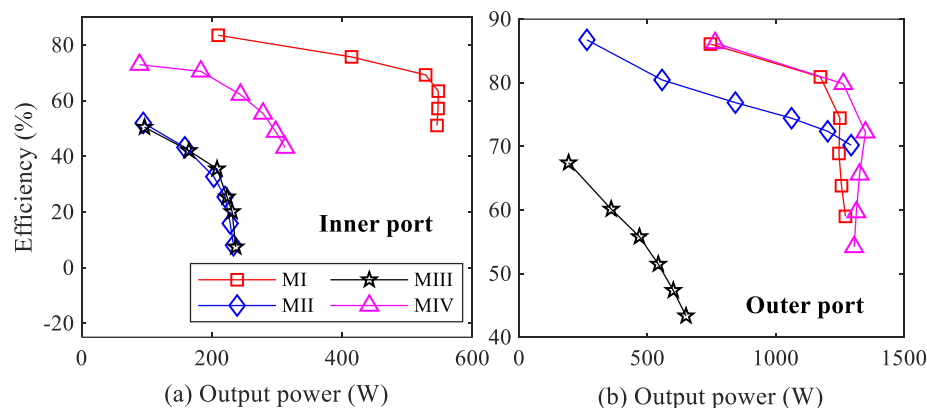


Figure 10. Variation in the output power with efficiency: (a) inner port and (b) outer port.

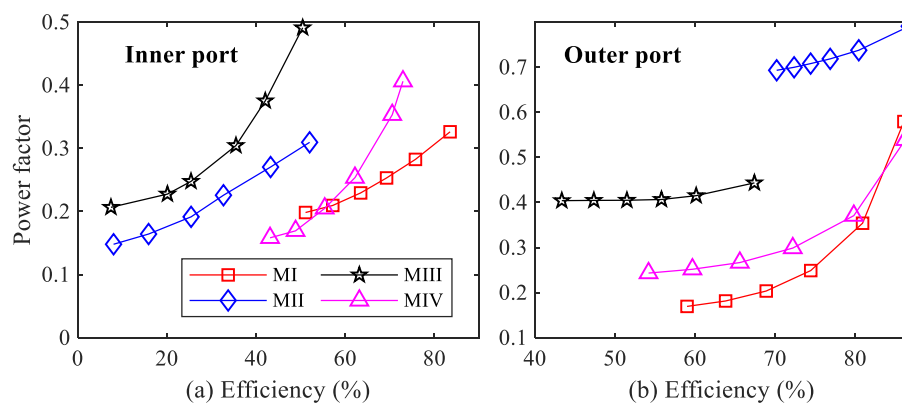


Figure 11. Variation in the power factor and efficiency: (a) inner port and (b) outer port.

Moreover, Figure 12 shows how output power changes with copper losses. Looking closely at Figure 12a, the inner port indicates that MI and MIV exhibit high output power and low copper losses. However, due to saturation, copper losses in MII and MIII increase at the detriment of the output power. Like Figure 12a, Figure 12b demonstrates that only MIII experiences substantial copper losses at a low output power in the outer port, whereas the other designs only experience moderate losses. Output power and efficiency were the two effects of copper losses that were most pronounced.

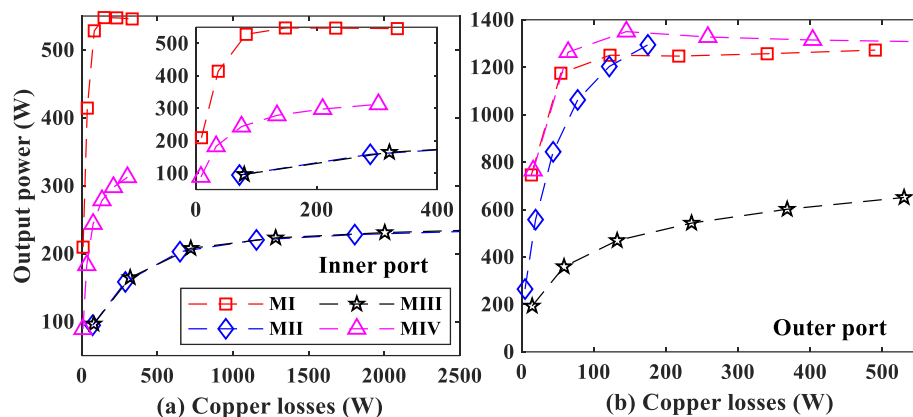


Figure 12. Variation in the output power and copper losses: (a) inner port and (b) outer port.

Figure 13 illustrates the analysis of the variation in total losses with efficiency. It is clear that efficiency declines when machine losses rise for both the inner and outer ports. It is also clear that MI offers excellent efficiency and fewer losses at the maximum output power. The maximum efficiency achieved for the inner machine is close to 80%, while the maximum efficiency for the outer machine is approaching 90%.

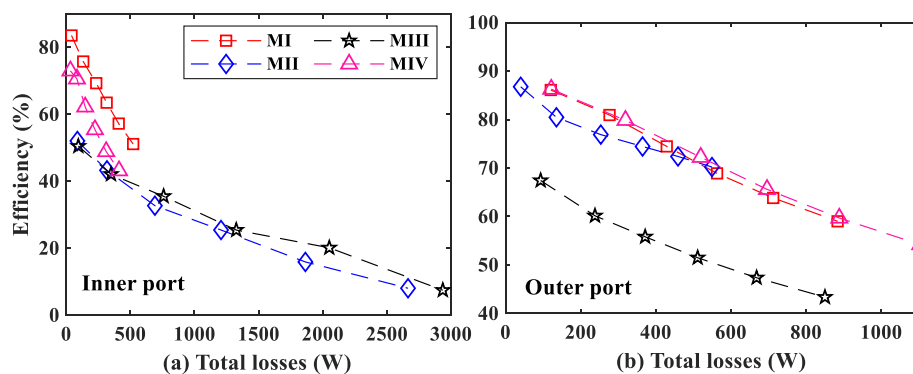


Figure 13. Variation in total machine losses and efficiency: (a) inner port and (b) outer port.

Thus, keeping in view the key performance indicators, a detailed comparative analysis was performed, as shown in Figure 14, whereas torque and power density based on magnet utilization are summarized in Table 2. Based on the comparative examination of the key performance indicators, it was found that MI is the optimal design configuration. Therefore, it was primed for fabrication to test the feasibility of the FEA predicted results.

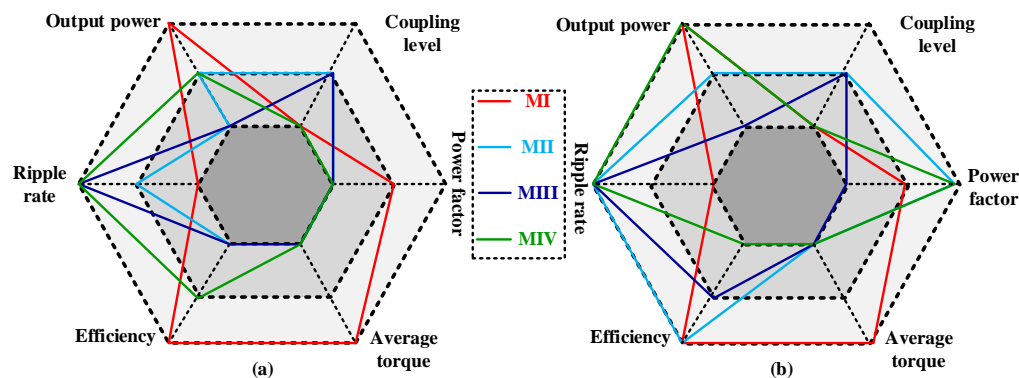


Figure 14. Detailed electromagnetic performance comparison for different slot/pole combinations: (a) inner machines and (b) outer machines.

Table 2. Rated torque and power density of inner and outer machines at current density = 15 A/mm².

	Torque Density (Nm/kg)			Power Density (kW/kg)		
	Inner Machine	Outer Machine	Cumulative	Inner Machine	Outer Machine	Cumulative
MI	9.3	22.11	31.41	1.47	3.47	4.94
MII	6.64	27.62	34.26	1.046	4.35	5.396
MIII	6.80	14.89	21.69	1.071	2.419	3.49
MIV	4.30	23.86	28.16	0.67	3.75	4.42

PM weight for MI and MIV = 0.36 kg, and PM weight for MII and MIII = 0.194 kg.

3.2. Experimental Verification

In order to validate the predicted FEA results, a test prototype was developed (as shown in Figure 15) utilizing the design parameters [15] illustrated in Figure 16 and listed in Table 3, with the lamination core material of 35H210 and paper insulation, whereas the test setup is shown in Figure 17. For counter rotation, the proposed CR-DRPMFSM was coupled to clockwise and counter-clockwise prime movers to independently rotate the inner and outer rotors. One of the prime movers runs clockwise, whereas the other runs counter-clockwise. To measure torque, a torque sensor and a speed sensor were coupled to the shaft of the rotor, and to record the electrical waveforms, an oscilloscope was used. The proposed design was tested under no-load for the back-EMF (as shown in Figure 18) and average torque (as shown in Figure 19) in both the inner and outer ports. It can be clearly seen that both the FEA and experimental test results fairly match. There is a slight deviation between the measured and FEA results, which is due to manufacturing tolerances and the nut-and-bolt holes.

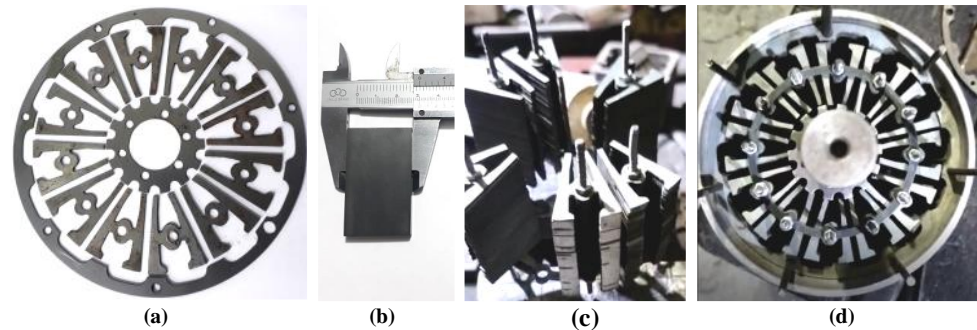


Figure 15. Hardware prototype development stages: (a) lamination sheets, (b) PM, (c) stator assembling process, and (d) final assembly.

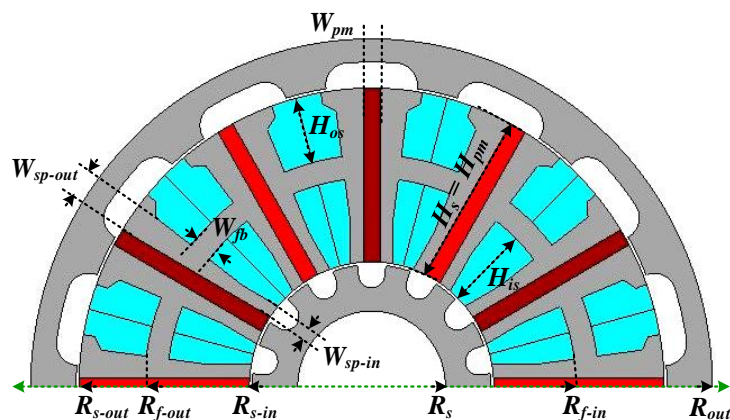


Figure 16. Leading design parameters for fabrication of prototype.

Table 3. Details of leading design parameters for fabrication of prototype.

Symbol	Value (mm)	Symbol	Value (mm)	Symbol	Value (mm)
R_{out}	60	R_{s-out}	51.5	R_{f-out}	41
R_{f-in}	35	R_{s-in}	21.5	R_s	13
W_{sp-in}	2.26	W_{sp-out}	3.75	W_{fb}	6
H_{is}	13.5	H_{os}	10.5	H_s	30
H_{pm}	30	W_{pm}	4		

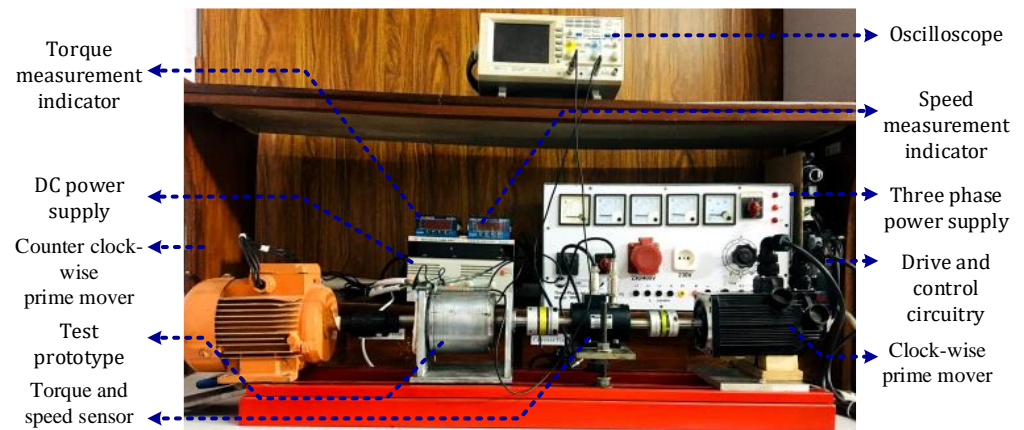


Figure 17. Test bench setup for proposed CR-DRPMFSM.

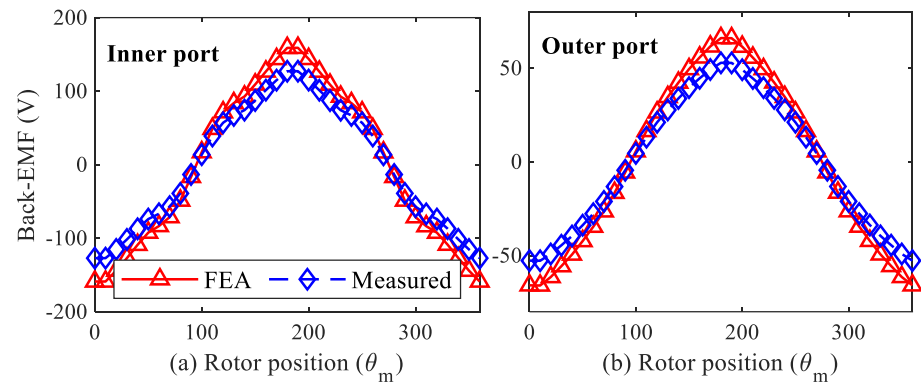


Figure 18. Measured and FEA results of back-EMF: (a) inner port and (b) outer port.

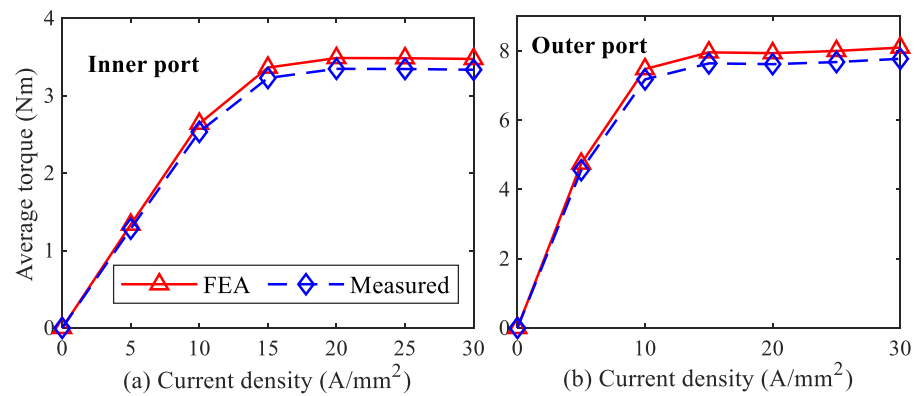


Figure 19. Measured and FEA results of average torque: (a) inner port and (b) outer port.

4. Conclusions

In this paper, the impact of series and parallel stator teeth on the electromagnetic performance of counter-rotating dual-rotor permanent-magnet flux-switching machines (CR-DRPMFSMs) was investigated. FEA was utilized to evaluate four machine configurations (MI, MII, MIII, and MIV) with different slot/pole combinations. The FEA no-load results demonstrate that MI topology has the highest flux linkage and lowest harmonic content for both the inner and outer ports. The back-EMF is most sinusoidal for MI and MIV in the inner port and MI in the outer port.

Under load, MI exhibits the highest average torque (15.5 Nm) and overload capability. MIV has comparable performance. The lowest torque ripple occurs with MI in both ports. MI also has the highest efficiency (80% inner and 90% outer).

Overall, MI with the 12S/14P-12S/14P configuration provides optimal electromagnetic performance by mitigating the magnetic coupling effects. This is attributed to the parallel stator teeth design. In contrast, MIII with the maximum coupling effects has the poorest performance.

A CR-DRPMFSM prototype based on the MI topology was constructed and tested. The experimental back-EMF and torque results validate the FEA predictions. In conclusion, this study provides a quantitative and in-depth investigation of magnetic coupling effects in CR-DRPMFSMs, demonstrating that the MI topology with parallel stator teeth maximizes performance. The findings contribute to the improved design of this emerging dual-port flux-modulation machine for direct-drive counter-rotating wind turbines.

Author Contributions: Conceptualization, W.U. and F.K.; methodology, W.U.; software, W.U.; validation, U.B.A., W.U. and F.K.; formal analysis, W.U., B.K. and S.A.K.; investigation, W.U. and B.K.; resources, F.K.; data curation, W.U., B.K. and S.A.K.; writing—original draft preparation, W.U.; writing—review and editing, U.B.A. and F.K.; visualization, W.U. and S.A.K.; supervision, F.K. and U.B.A. All authors have read and agreed to the published version of the manuscript.

Funding: This research received no external funding.

Data Availability Statement: The data that support the findings of this study are available from the corresponding author upon request. The data are not publicly available due to privacy or ethical restrictions.

Conflicts of Interest: The authors declare no conflict of interest.

References

1. Ullah, W.; Khan, F.; Hussain, S. Investigation of Inner/Outer Rotor Permanent Magnet Flux Switching Generator for Wind Turbine Applications. *IEEE Access* **2021**, *9*, 149110–149117. [[CrossRef](#)]
2. Kwon, J.W.; Kwon, B.I. Design of novel high performance dual rotor flux-switching drum winding machine. *J. Electr. Eng. Technol.* **2019**, *14*, 2019–2025. [[CrossRef](#)]
3. Zhao, G.; Li, Z.; Hua, W.; Ding, S.; Su, P.; Jiang, X. Analysis of a Novel Dual-Three-Phase Dual-Rotor Flux-Switching Permanent Magnet Machine. In Proceedings of the IEEE 20th Biennial Conference on Electromagnetic Field Computation (CEFC), Denver, CO, USA, 24–26 October 2022; pp. 1–2.
4. Wang, Y.; Zhao, W.; Yu, M.; Yang, Y.; Kwon, B.-I. Design and Optimization of a Novel Dual-Stator Flux-Switching Permanent Magnet Machine. In Proceedings of the IEEE 3rd Student Conference on Electrical Machines and Systems (SCEMS), Jinan, China, 4–6 December 2020; pp. 89–93.
5. Xiang, Z.; Quan, L.; Zhu, X.; Huang, J.; Fan, D. Investigation of Optimal Split Ratio in Brushless Dual-Rotor Flux-Switching Permanent Magnet Machine Considering Power Allocation. *IEEE Trans. Magn.* **2018**, *54*, 8102104. [[CrossRef](#)]
6. Yu, C.; Niu, S.; Ho, S.L.; Fu, W.N. Design and analysis of a magnetless double-rotor flux switching motor for low cost application. *IEEE Trans. Magn.* **2014**, *50*, 8105104. [[CrossRef](#)]
7. Selema, A. Development of a Three-Phase Dual-Rotor Magnetless Flux Switching Generator for Low Power Wind Turbines. *IEEE Trans. Energy Convers.* **2020**, *35*, 828–836. [[CrossRef](#)]
8. Saeed, M.S.; Mohamed, E.E.; Sayed, M.A. Design and analysis of dual rotor multi-tooth flux switching machine for wind power generation. In Proceedings of the 2016 Eighteenth International Middle East Power Systems Conference (MEPCON), Cairo, Egypt, 27–29 December 2016; pp. 499–505.
9. Li, X.; Liu, S.; Wang, Y. Design and Analysis of a New HTS Dual-Rotor Flux-Switching Machine. *IEEE Trans. Appl. Supercond.* **2017**, *27*, 5200605. [[CrossRef](#)]

10. Zhao, X.; Niu, S.; Fu, W. Design of a novel parallel-hybrid-excited dual-PM machine based on armature harmonics diversity for electric vehicle propulsion. *IEEE Trans. Energy Con.* **2019**, *66*, 4209–4219. [[CrossRef](#)]
11. Hassannia, A. Conceptual design of fractional slot concentrated winding dual-rotor double-speed synchronous motor. *IEEE Trans. Energy Convers.* **2020**, *35*, 986–993. [[CrossRef](#)]
12. Du, J.; Xue, Y.; Yang, X. Modeling and inner–outer decoupling of dual-rotor machines for continuous variable transmission systems. *IEEE Trans. Ind. Electron.* **2017**, *64*, 8472–8483. [[CrossRef](#)]
13. Xiang, Z.; Lu, Z.; Zhu, X.; Jiang, M.; Fan, D.; Quan, L. Research on magnetic coupling characteristic of a double rotor flux-switching PM machine from the perspective of air-gap harmonic groups. *IEEE Trans. Ind. Electron.* **2022**, *69*, 12551–12563. [[CrossRef](#)]
14. Zhou, L.; Hua, W. Influences of stator teeth number on PM coupling levels of co-axial dual-mechanical-port flux-switching PM machines. *IEEE Trans. Magn.* **2019**, *55*, 1–7. [[CrossRef](#)]
15. Ullah, W.; Khan, F.; Akuru, U.B.; Yousuf, M. Magnetic Coupling Effect and Performance Analysis of Dual Rotor Permanent Magnet Flux Switching Generator for Counter Rotating Wind Power Generation. *IEEE Trans. Energy Convers.* **2023**, 1–13. [[CrossRef](#)]

Disclaimer/Publisher’s Note: The statements, opinions and data contained in all publications are solely those of the individual author(s) and contributor(s) and not of MDPI and/or the editor(s). MDPI and/or the editor(s) disclaim responsibility for any injury to people or property resulting from any ideas, methods, instructions or products referred to in the content.